8-26-2011

Crystal structure of plasminogen activator inhibitor-1 in an active conformation with normal thermodynamic stability

Jan K. Jensen
Aarhus Universitet

Lawrence C. Thompson
The University of Tennessee, Knoxville

Joel C. Bucci
The University of Tennessee, Knoxville

Poul Nissen
Aarhus Universitet

Peter G.W. Gettins
University of Illinois at Chicago

See next page for additional authors

Recommended Citation

Jensen, J., Thompson, L., Bucci, J., Nissen, P., Gettins, P., Peterson, C., Andreasen, P., & Morth, J. (2011). Crystal structure of plasminogen activator inhibitor-1 in an active conformation with normal thermodynamic stability. *Journal of Biological Chemistry, 286* (34), 29709-29717. https://doi.org/10.1074/jbc.M111.236554

THE JOURNAL OF BIOLOGICAL CHEMISTRY VOL. 286, NO. 34, pp. 29709–29717, August 26, 2011

Crystal Structure of Plasminogen Activator Inhibitor-1 in an Active Conformation with Normal Thermodynamic Stability*[S]

Received for publication, March 3, 2011, and in revised form, May 29, 2011 Published, JBC Papers in Press, June 21, 2011, DOI 10.1074/jbc.M111.236554

Jan K. Jensen[‡§1,2], Lawrence C. Thompson[¶], Joel C. Bucci[¶], Poul Nissen[‡‖], Peter G. W. Gettins[**], Cynthia B. Peterson[¶], Peter A. Andreasen[‡§], and J. Preben Morth[‡‖‡‡1,3]

From the [‡]Department of Molecular Biology, [§]Danish-Chinese Center for Proteases and Cancer, and [‖]Center for Structural Biology, Aarhus University, 8000 Aarhus C, Denmark, the [¶]Department of Biochemistry and Cellular and Molecular Biology, University of Tennessee, Knoxville, Tennessee 37996, [**]Department of Biochemistry and Molecular Genetics, University of Illinois at Chicago, Chicago, Illinois 60607, and the [‡‡]Centre for Molecular Medicine, Nordic EMBL Partnership, University of Oslo, 0318 Oslo, Norway

The serpin plasminogen activator inhibitor-1 (PAI-1) is a crucial regulator in fibrinolysis and tissue remodeling. PAI-1 has been associated with several pathological conditions and is a validated prognostic marker in human cancers. However, structural information about the native inhibitory form of PAI-1 has been elusive because of its inherent conformational instability and rapid conversion to a latent, inactive structure. Here we report the crystal structure of PAI-1 W175F at 2.3 Å resolution as the first model of the metastable native molecule. Structural comparison with a quadruple mutant (14-1B) previously used as representative of the active state uncovered key differences. The most striking differences occur near the region that houses three of the four mutations in the 14-1B PAI-1 structure. Prominent changes are localized within a loop connecting β-strand 3A with the F helix, in which a previously observed 3_{10}-helix is absent in the new structure. Notably these structural changes are found near the binding site for the cofactor vitronectin. Because vitronectin is the only known physiological regulator of PAI-1 that slows down the latency conversion, the structure of this region is important. Furthermore, the previously identified chloride-binding site close to the F-helix is absent from the present structure and likely to be artifactual, because of its dependence on the 14-1B mutations. Instead we found a different chlorine-binding site that is likely to be present in wild type PAI-1 and that more satisfactorily accounts for the chlorine stabilizing effect on PAI-1.

Plasminogen activator inhibitor-1 (PAI-1)[4] is a specific and fast-acting inhibitor of each of the two plasminogen activators, tissue type (tPA) and urokinase type plasminogen activator and thus an inhibitor of plasmin-mediated fibrinolysis and tissue remodeling. Since its discovery in the mid-1980s, this member of the serpin family has been intensely studied to achieve an in-depth understanding of its physiological and pathophysiological functions (for a review see Ref. 1). PAI-1 has been directly implicated in cardiovascular diseases and cancer and is a potential therapeutic target (for reviews see Refs. 2 and 3). In addition to the target proteases, PAI-1 also binds to endocytosis receptors of the low density lipoprotein receptor family and the extracellular matrix glycoprotein vitronectin (for a review, see Ref. 1). To better understand these molecular interactions, many loss-of-function or loss-of-interaction mutants have been constructed (4).

Central to the protease inhibition mechanism is the 20-residue surface-exposed loop called the reactive center loop (RCL) that initially interacts with the target serine protease in the same way as a substrate. Following the initial protease cleavage, the N-terminal part of the RCL inserts as strand 4 in β-sheet A (s4A), the central sheet in PAI-1, translocating the covalently linked protease to the opposite pole of the serpin and thereby trapping it in an inactive covalent complex. The insertion of the RCL into β-sheet A is believed to release energy needed to drive the inhibitory mechanism, converting the serpin into the thermodynamically most stable form (5, 6). Under certain conditions, PAI-1 exhibits "substrate behavior," during which the active protease is prematurely released prior to RCL insertion, leaving the serpin in an inactive protease-cleaved form (for reviews, see Refs. 1 and 4).

PAI-1 shares a unique functional feature among less than a handful of serpins in its ability to spontaneously insert the RCL into β-sheet A without prior cleavage with a half-life of 1–2 h at 37 °C, resulting in a thermodynamically more stable and non-inhibitory state, termed the latent form (7). The physiological function of latency transition is still uncertain but may serve as a protection against long term anti-fibrinolytic actions of PAI-1. Latency transition adds an experimental challenge for time extensive *in vitro* and *in vivo* assays on PAI-1 or when growing protein crystals.

In 1995, a quadruply mutated (N150H, K154T, Q319L, and M354I) PAI-1 termed 14-1B was isolated by random mutagenesis screens. The conversion of 14-1B to the latent state at 37 °C was delayed by more than 70-fold. In addition, 14-1B exhibits a large increase in thermodynamic stability, manifested by a

* This work was supported by a center of excellence grant from the Danish National Research Foundation (to P. A. A. and P. N.) and by American Heart Association Grant 10GRNT4430033 (to C. B. P.).

[S] The on-line version of this article (available at http://www.jbc.org) contains supplemental Tables S1 and S2 and Figs. S1 and S2.

The atomic coordinates and structure factors (codes 3Q02 and 3Q03) have been deposited in the Protein Data Bank, Research Collaboratory for Structural Bioinformatics, Rutgers University, New Brunswick, NJ (http://www.rcsb.org/).

[1] Supported by the Lundbeck Foundation.

[2] To whom correspondence should be addressed. Tel.: 4589425289; Fax: 4586123178; E-mail: jkj@mb.au.dk.

[3] Supported by Carlsbergfondet.

[4] The abbreviations used are: PAI-1, plasminogen activator inhibitor-1; DSC, differential scanning calorimetry; RCL, reactive center loop; tPA, tissue type plasminogen activator; MES, 4-morpholineethanesulfonic acid; PDB, Protein Data Bank.

10 °C increase in the denaturation temperature (8). The first x-ray crystal structure of active PAI-1 was determined with 14-1B at a resolution of 3 Å (9). The structure featured the same overall fold as other inhibitory serpins (for a review, see Ref. 10). Higher resolution structures of active 14-1B have since been determined (see supplemental Table S1), with resolutions of 2.7 (11) and 2.4 Å (12), respectively. Because 14-1B retained inhibitory activity toward the target proteases, the x-ray crystal structure analysis of 14-1B has provided the basis for many biochemical investigations of active PAI-1, including the mapping of sites for molecular interactions and interpreting functional effects caused by single or multiple mutations in PAI-1 (4). However, accumulating evidence has raised questions about the validity of using 14-1B as a valid representative of the wild type protein (13–16). As examples, 14-1B was observed to differ from native PAI-1 when analyzing the binding of a set of conformational specific antibodies (14) and when studying the ability of PAI-1 to induce multimerization of its cofactor vitronectin (16).

In a study designed to dissect the contributions to the intrinsic fluorescence from each of the four Trp residues in human PAI-1, Trp^{175}, which is highly conserved among serpins, was substituted with a Phe. In addition to a small increase in substrate behavior when reacting with tPA and an only 3.5-fold delayed latency transition ($t_{½}$ = ~7 h, 37 °C), W175F behaved similarly to wild type PAI-1 with regard to all tested biochemical functions (17). The mutated residue is centered in the "breach" region, where β-sheet A opens to allow the insertion of the first residue of the RCL. Residue 175 was shown to be important for the regulation of the rate of insertion of the first few residues of the RCL (17).

Here we report the crystal structure of PAI-1 W175F at 2.3 Å resolution. We were able to identify a previously unknown chloride site that leads to a revised hypothesis of how elevated salt concentrations stabilize the inhibitory activity of PAI-1. Furthermore, two novel binding sites for Zn^{2+} were identified that likely contribute to the reported affinity of PAI-1 for divalent metal ions. We demonstrate that W175F PAI-1 has a thermodynamic stability comparable with that of active wild type PAI-1. In accordance with this, the structural analysis provides evidence that a single substitution does not impose significant structural deviations from the wild type conformation. Comparison with the current structural model of active PAI-1 reveals significant structural differences with biochemical implications. We believe that our new structure represents a correct model for the metastable active form of PAI-1, thus providing some missing key information that enhances the structural characterization of the active form. Our observations also provide evidence that the thermodynamic stability of serpins is not the only determinant of the rate of RCL insertion.

EXPERIMENTAL PROCEDURES

W175F PAI-1 Protein Expression—A pET-24d expression vector (Novagen) containing the human PAI-1 full-length DNA sequence (from the N-terminal ^{1}VHHPPS^{6}) without any tags was a kind gift from Grant E. Blouse. The W175F substitution was created by site-directed mutagenesis according to the QuikChange protocol (Stratagene). Rosetta2 BL21 (DE3) pLysS cells were transformed with the vector and grown at 30 °C while agitating in LB medium supplemented with 50 μg/ml kanamycin and 34 μg/ml chloramphenicol until an optical density at 600 nm of ~1 was reached. The temperature was reduced to 15 °C, and the cell culture was allowed to cool for 2 h before protein expression was induced by adding isopropyl β-D-1-thiogalactopyranoside to a final concentration of 1 mM. After an overnight incubation at 15 °C, the cells were harvested by centrifugation and stored in pellet form at −80 °C until protein purification.

Purification of W175F PAI-1 Protein—Cell pellets were resuspended in 50 mM NaH_2PO_4, pH 6.5, 1 mM EDTA, and 10 mg of Sigma protease inhibitor mixture P8465 was added per gram of pellet. The cells were lysed by sonication on ice, and the supernatant containing soluble W175F PAI-1 protein was cleared by centrifugation. The following was all performed at 4 °C. The supernatant was loaded onto a SP Sepharose FF column and washed extensively with 50 mM NaH_2PO_4, pH 6.5, 80 mM $(NH_4)_2SO_4$, and 1 mM EDTA, and bound protein was eluted with a linear gradient of 80–500 mM $(NH_4)_2SO_4$. PAI-1-containing fractions (high concentrations of $(NH_4)_2SO_4$) were pooled and dialyzed overnight against 50 mM NaH_2PO_4, pH 7.0, 500 mM NaCl, and 20 mM imidazole and subsequently loaded onto a chelating Sepharose FF column charged with nickel. The column was then washed and eluted with a 20–120 mM imidazole gradient. Fractions were captured into NaH_2PO_4, pH 6.25, NaCl, and EDTA (final [EDTA] = 5 mM). The PAI-1 containing fractions were pooled, concentrated, and loaded onto a 2.5 × 115 cm high resolution Sephacryl S-100 column extensively equilibrated in 50 mM NaH_2PO_4, pH 6.25, 300 mM NaCl, and 1 mM EDTA. W175F PAI-1 eluted as a single peak, the fractions of which were pooled, concentrated, and stored at −80 °C. Protein purity better than 95% was confirmed by Coomassie Brilliant Blue-stained reducing SDS-PAGE, and the identity was confirmed by Western blot and MALDI-MS. Protein concentration was determined by measuring the optical density at 280 nm using ϵ_{280} = 0.70 ml·mg^{-1}·cm^{-1} and a molecular weight of 42,730 (both calculated using the ProtParam tool at the ExPASy Bioinformatics Resource Portal). The strategy of employing a low temperature during expressing ensures that only an insignificant amount of latent W175F PAI-1 protein is present in the preparations.

PAI-1 Stability Assay—The inhibitory activity of the PAI-1 preparation was tested by titration with tc-tPA. The relative amount of functional tPA was determined using a chromogenic assay by the addition of 1 mM Spectrozyme tPA (American Diagnostica Inc). The release of free *p*-nitroaniline upon cleavage of the substrate by tPA was monitored at 405 nM. Typical PAI-1 preparations were ≥85% active. The rate of conversion of PAI-1 to the latent form was determined essentially as described previously (14). A sample of 100 nM PAI-1 was equilibrated in 20 mM HEPES, pH 7.4, containing 1% BSA at 37 °C. Sodium halide solutions (NaCl, NaF, or NaBr) were added to a final concentration of either 150 mM or 1.0 M. Over time, aliquots were mixed with active tPA at a final concentration of 50 nM PAI-1 and 60 nM tPA. Relative PAI-1 activity was normalized and fit to a single exponential to determine k_{lat}, the rate

constant for conversion to the latent form. The data are the averages of three separate experiments.

Thermal Stability Monitored by CD Spectroscopy and Differential Scanning Calorimetry—Thermal denaturation of PAI-1 by CD spectroscopy was performed on a JASCO-810 circular dichroism system, equipped with Peltier temperature-controlled cuvette holder. The change in CD signal was followed at 222 nm while heating a 1-cm cuvette containing 10 μg/ml PAI-1 in 0.1 °C steps from 35–75 °C at a ramp speed of 50 °C/h under mild agitation. Denaturation curves were an average of three independent experiments, corrected for buffer scan and normalized to 1. Melting point temperatures (T_m) were obtained from the inflection point of the sigmoid curves by nonlinear fit of the data as described (18). Native and 14-1B *Escherichia coli* PAI-1, used for comparison, was prepared in a similar way as described above. Latent PAI-1 was prepared by incubating the native PAI-1 sample at 37 °C for >24 h prior to the CD experiment. All of the samples were prepared in 50 mM NaH_2PO_4, pH 6.6. Thermal denaturation of PAI-1 by differential scanning calorimeter (DSC) was performed on a MicroCal VP-DSC. The DSC curves were obtained by heating the sample and reference cell from 20 to 90 °C at a rate of 90 °C/h. Protein samples were prepared by dialysis against 50 mM NaH_2PO_4, pH 6.6, supplemented with 500 mM NaCl to prevent protein precipitation at the PAI-1 concentrations of ~0.8 mg/ml required for the DSC measurement.

Crystallization of W175F PAI-1—Protein sample and crystallization conditions from the previous crystallization study of 14-1B PAI-1 (12) were chosen as the starting point for crystallization of W175F PAI-1. In parallel crystallization trials with the available sparse matrix screens, kits from Hampton were performed; these screens, however, did not yield any crystals of diffraction quality. W175F PAI-1 protein sample was buffer-exchanged into crystallization buffer (20 mM MES, pH 6.1, 500 mM NaCl) to a final concentration of 11 mg/ml. Crystals appeared within 2 weeks at 18 °C by hanging drop vapor diffusion against a reservoir of 0.5 ml 0.5–3.0 M NaCl. The data were collected at 100 K.

Cryoprotection—Crystals were cryoprotected either by quick (10–30 s) soak in a drop of well solution supplemented with 25% ethylene glycol supplemented with 0.5 M NaCl or by adding ethylene glycol directly to the drop containing crystals. The later procedure was done by first adding ethylene glycol to a concentration of ~12.5% following 20 min of incubation before further addition to a concentration of ~19% allowing additional ~2-h incubation. Crystals were mounted in 0.05–0.2-mm nylon loops (Hampton) and snap-frozen in liquid nitrogen or directly in the nitrogen cryostream at the beamline.

Diffraction Data Collection and Processing—A native data set to 2.3 Å resolution was collected at 100 K on the end station X06SA at the Swiss Light Source (SLS) in Villingen at a wavelength of 1.001 Å (data set 1). A long wavelength data set at the zinc edge was carried out at 1.280 Å on the end station X12 at EMBL Hamburg (data set 2). On-site software was used to validate the crystal diffraction quality as well as preliminary indexing of data from the individual crystals. The data set 1 and 2 were indexed, integrated, and scaled in space group $P2_1$ using the XDS program package (19) (see Table 1). The final structure factor files were prepared using XDSCONV (XDS program package) and subroutines in the CCP4 suite (20).

Structure Determination and Refinement—The initial phases were obtained by molecular replacement with (PDB code 1DVM) as search model, refinement, and validation with programs within the PHENIX program package (21). Model building was performed in COOT (22). Structure figures were prepared using the PyMOL molecular graphics system (version 1.2r3pre).

RESULTS

W175F Has Wild Type Thermodynamic Stability—It was previously shown that the 14-1B PAI-1 variant exhibited a more than 70-fold increased functional stability as well as a large increase in thermal stability, both indicative of a structure decisively different from that of wild type PAI-1. To investigate the effects of the more modest side chain alteration in the W175F variant, its thermal stability was determined by CD spectroscopy. The denaturing temperature for W175F was determined to be 50.8 ± 0.4 °C (Fig. 1*A* and supplemental Fig. S1), indistinguishable from the 50.2 ± 0.3 °C of active wild type PAI-1 ($p = 0.1062$, Students' t test). Both values were significantly lower than those observed for 14-1B (59.7 ± 0.3 °C, $p < 0.0001$, Students' t test) and latent wild type (68.1 ± 0.4 °C, $p < 0.0001$). Importantly, the melting point temperatures of active and latent wild type PAI-1 as well as of active 14-1B agreed well with previously published data (8, 18).

To confirm the observed melting point temperatures (T_m) of the three PAI-1 samples by an independent method, we used DSC. Although it was necessary to increase the NaCl concentration to 500 mM to maintain the elevated protein concentration needed for a DSC experiment (~0.8 mg/ml), the observed melting point temperatures were comparable with those determined by CD. The denaturation temperature of W175F was indistinguishable from active wild type PAI-1 with peaks centered at ~52 °C (Fig. 1*B*). Consistent with the CD measurements, 14-1B denatured in the calorimeter at a temperature >12 degrees higher than both wild type and W175F PAI-1, with a T_m value between 65 and 67 °C.

During all thermal melting experiments using either CD or DSC, denaturation of PAI-1 was accompanied by bulk precipitation of the sample protein. For the DSC experiments with 14-1B PAI-1, this irreversible unfolding skewed the shape of the transition point peak and the postdenaturation baseline. This perturbed peak shape prevented the determination of a precise T_m. This protein precipitation above the melting temperatures precluded a full thermodynamic analysis of the unfolding/folding process. Nonetheless, these striking thermal stability data prompted us to pursue three-dimensional structure determination on W175F as a model for the metastable active structure of PAI-1.

Initial Structural Observations—The combination of a slightly delayed rate of latency transition rate and an optimized expression and purification protocol helped to maintain the active conformation of W175F during preparation and crystallization. Protein crystals grew readily from conditions similar to those previously reported for 14-1B PAI-1 (12). Two data sets were used for refinement (Table 1). Data set 1 at 2.3 Å resolu-

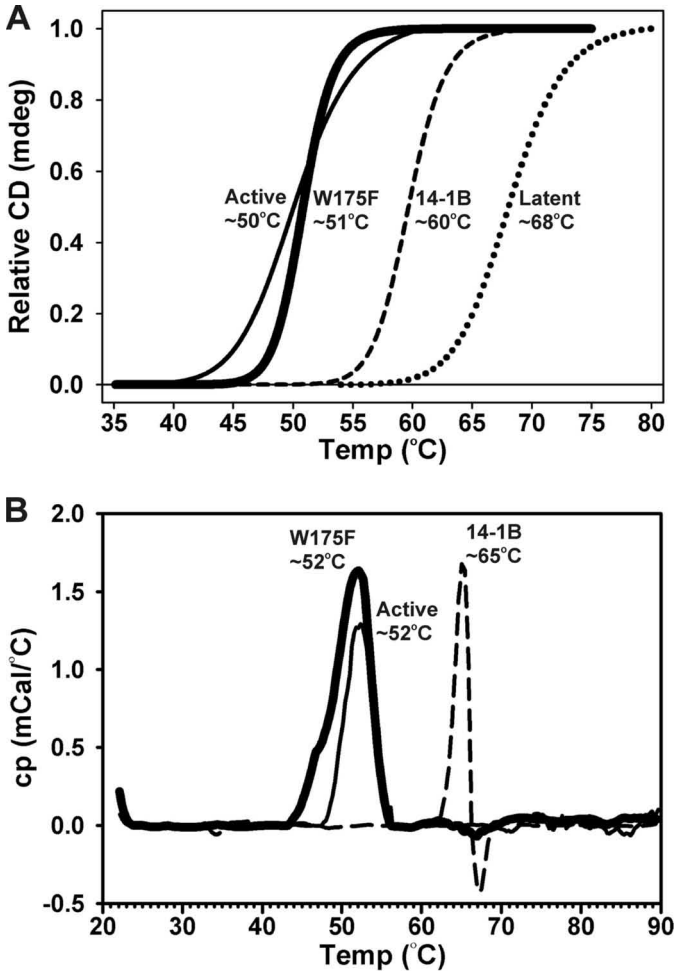

FIGURE 1. **Thermal denaturation experiments by CD and DSC.** *A*, CD thermal denaturation profiles of the indicated PAI-1 variants are represented by the curves from fits using equation 1 to the raw data for active W175F (*thick solid line*), active 14-1B (*broken line*), or active (*thin line*) and latent (*dotted line*) wild type PAI-1. The data correspond to the normalized change in CD signal of the respective samples as a function of temperature. Denaturation temperatures, averaged from three independent measurements, are given by the labels on the corresponding curves. *B*, DSC curves of active W175F (*thick solid line*), active wild type (*thin line*), and active 14-1B PAI-1 (*broken line*). The melting point temperature of the protein corresponding to the midpoint of the thermal transition peak in each individual DSC curve is given as a label to the corresponding peak.

tion formed the basis for the main structural analysis, whereas data set 2 at 2.6 Å resolution was collected at a low energy wavelength above the Zn^{2+} and Cu^{2+} edge ($\lambda = 1.5$) to allow reliable identification of atoms with anomalous scattering in the difference Fourier map. We attribute the higher refinement statistics for data set 1 (R_{work} and R_{free}) to the accumulation of radiation damage introduced during data collection at the Swiss light source, because of the higher x-ray brilliance. It should be noted that only a few crystals diffracted to 2.3 Å. These crystals were small in size (~40 × 40 × 40 μm), leaving the crystal completely bathed in x-rays throughout the entire exposure, resulting in increased radiation damage as compared with crystals larger than the x-ray beam. Larger crystals will in principal include nonradiated crystal for the initial 180 degrees of exposure. It is noteworthy that this crystal form crystallizes in a different space group and with different unit cell parameters as compared with the previous 14-1B crystals (see supple-

TABLE 1
Data collection and refinement statistics

Protein Data Bank code	3Q02	3Q03
Data collection	Data set 1	Data set 2
Synchrotron	SLS Villingen	EMBL Hamburg
Beamline	PX06SA	X12
Wavelength (Å)	1.00	1.28
Resolution range (Å)[a]	30–2.29 (2.39–2.3)	30–2.6 (2.75–2.64)
Space group	$P2_1$	$P2_1$
Unit cell dimensions		
a, *b*, *c* (Å)	77.44, 67.17, 90.36	76.68, 67.16, 91.16
α, β, γ (°)	90.0, 98.5, 90.0	90.0, 100.5, 90.0
Mosaicity (°)	0.14	0.17
Unique reflections[a]	40,531 (4366)	52,134 (6049)
Completeness (%)[a]	98.7 (97.9)	99.1 (99.6)
Redundancy [a]	4.7 (4.6)	3.2 (3.2)
R_{meas} (%)[a,b]	5.2 (70.6)	9.1 (58.4)
$I/\sigma I$ [a]	17.61 (2.10)	11.19 (2.03)
Wilson *B*-factor	57.5	48.4
Refinement		
Resolution range (Å)[a]	20–2.3 (2.39–2.3)	20–2.64 (2.68–2.64)
R_{work} (%)[c]	19. 1	17.2
R_{free} (%)[d]	23.8	22.5
Atomic model		
Protein atoms	5770	5791
Ions		
Cl^-	2	2
Zn^{2+}	2	2
Other ligand	1	
Water molecules	145	247
Root mean square deviations[e]		
Bond lengths (Å)	0.029	0.006
Bond angles (°)	2.525	1.186
Ramachandran favored	96.77%	96.37%
Ramachandran allowed	3.09%	3.63%
Ramachandran outliers	0.14%	0.00%

[a] The values in parentheses indicate the shell of highest resolution.
[b] $R_{meas} = \Sigma_{hkl} (N/(N-1))^{1/2} \Sigma_i |I_{i,hkl} - \langle I_{hkl} \rangle| / \Sigma_{hkl} \Sigma_i |I_{i,hkl}|$.
[c] $R_{work} = \Sigma_{hkl} |F_{obs} - F_{calc}| / \Sigma_{hkl} |F_{obs}|$.
[d] R_{free} is calculated like R_{work} but from 5% (random subset) of the reflections excluded from the refinement.
[e] From ideal values.

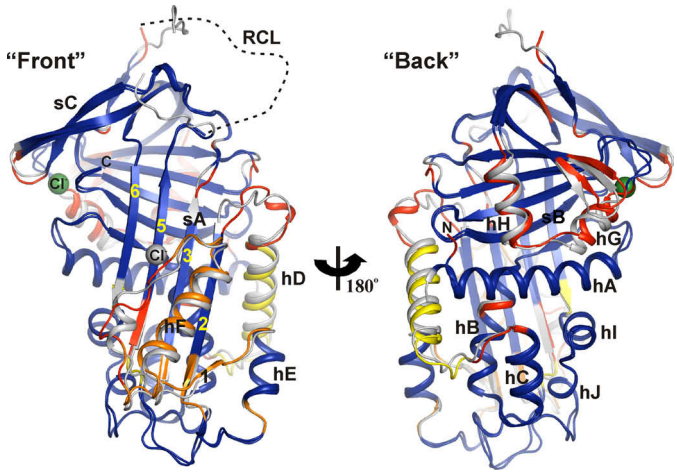

FIGURE 2. **Structure of active W175F PAI-1.** The results of the x-ray crystallography are shown in a front and back cartoon representation oriented with the central β-sheet A in the plane of the paper and the RCL toward the *top*. The structure is overlaid with the 14-1B structure shown in *gray* cartoon (PDB code 1DVM) by alignment using statistical alignment algorithms in RAPIDO. Invariant regions are colored in *blue* and regions deviating statistically color-scaled *yellow*, *orange*, or *red* according to increasing deviations between the structures. The chloride-binding sites in the W175F and 14-1B structures are highlighted by *green* or *gray spheres*, respectively. Secondary structure elements (α-helix (*h*) and β-sheet (*s*)) are labeled, and the specific numbering of strands 1–3, 5, and 6 of sA is shown. The RCL is sketched with a hypothetical *dashed black line* replacing the missing main chain in the W175F structure.

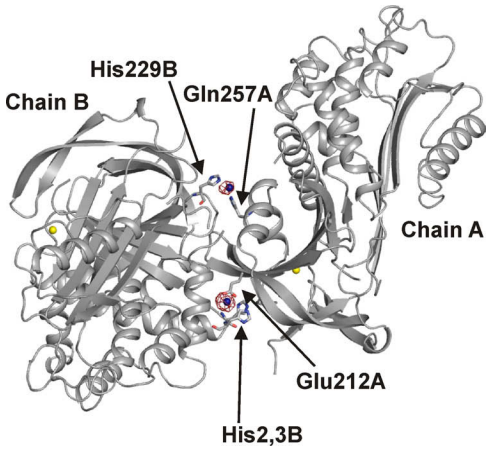

FIGURE 3. **Cartoon drawing of the crystal asymmetry unit containing two molecules of W175F chain A and B.** The positions of Cl^- and Zn^{2+} ions are marked with *yellow* and *blue spheres*, respectively. The electron density of the two Zn^{2+} ions is contoured at 3.0 sigma (*red mesh*) in the difference Fourier map. Residues in coordinating distance to the Zn^{2+} ions are highlighted as *sticks* and labeled by *arrows* and *text*.

mental Table 1). The final model (Fig. 2) is more than 95% complete and shares the common overall fold of an active serpin observed with other inhibitory members of the family. As expected, the electron density of the solvent-exposed flexible RCL (Ser^{331}–Pro^{349}) is missing and reflects the ability of the RCL to adopt different conformations suitable for the interaction with target proteases (10). Strong peaks in the difference map of data set 2 clearly identify two Zn^{2+} sites bridging the two PAI-1 molecules in the asymmetric unit. The strongest site is coordinated by the two N-terminal histidine residues 2 and 3 (Fig. 3). Furthermore, the difference maps reveal the localization of a previously unknown halide-binding site (Figs. 2 and 4).

Chloride-binding Site in the Gate Region—From the anomalous diffraction data, it was evident that a strong, well defined chloride-binding site was located in the center of the functionally important "gate" region (Fig. 2), the region through which the unbroken main chain extracted from β-sheet C must pass to allow the complete insertion of the RCL in β-sheet A during latency transition. From a mechanistic point of view, the chloride atom could act as a gatekeeper by bridging several structural elements situated between the s3C/s4C loop and the loop

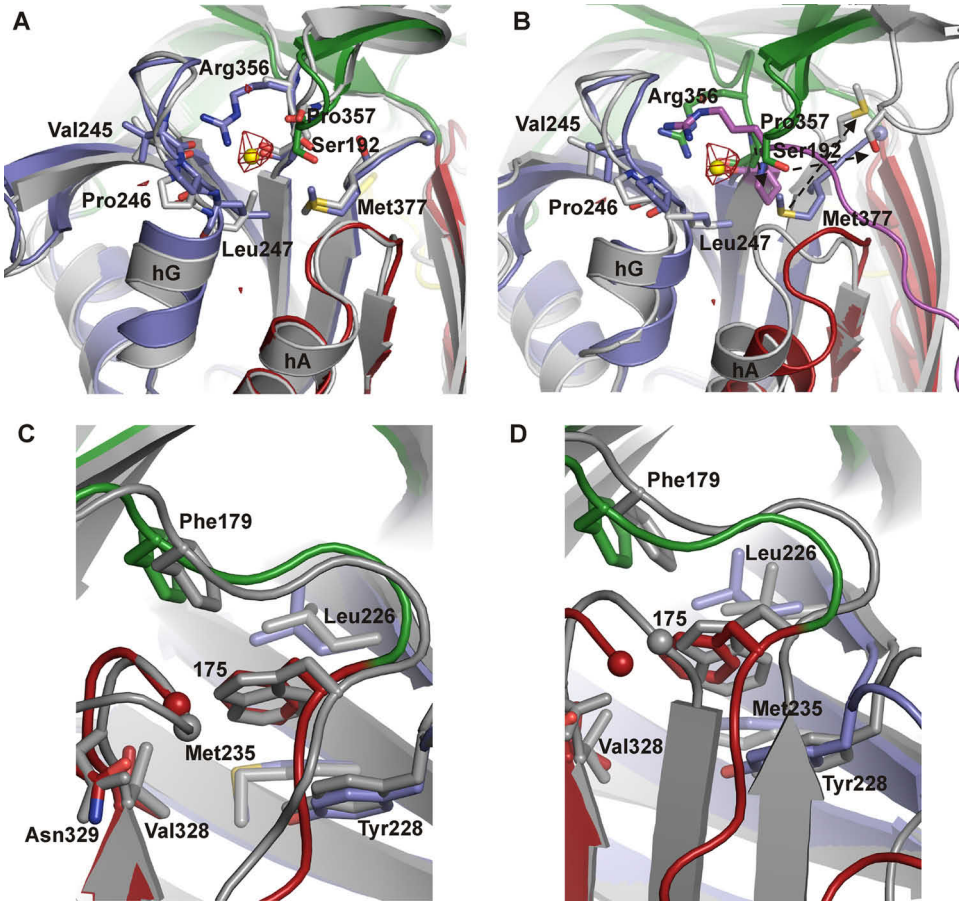

FIGURE 4. *Top panel*, close-up view of the chloride-binding site centered in the gate region. Side chains within 5 Å of the Cl^- ion are shown as *sticks* with corresponding residue labels. Alignments are shown with 14-1B structure (*gray*, PDB code 1DVM, *A*) and latent wild type PAI-1 (*gray*, PDB code 1LJ5, *B*). The electron density of the chloride is contoured at 3.0 sigma (*red mesh*) in the difference Fourier map. *Arrows* mark position changes of highlighted side chains during latency transition. The loop strand extracted from β-sheet C during latency transition with the pivotal point at Pro^{357} extending to the *bottom right* of the figure is marked in the latent structure with *magenta*. The Arg^{356} side chain is missing in the 14-1B structure. *Bottom panel*, a close-up representation of the mutated position 175 in the upper part of the breach region. Neighboring side chains within 5 Å of Phe^{175} are depicted as *sticks* with corresponding residue labels. Statistically calculated alignments in RAPIDO are shown with 14-1B structure (*gray*, PDB code 1DVM, *C*) and latent wild type PAI-1 (*gray*, PDB code 1LJ5, *D*). *Arrows* mark position changes of highlighted side chains during latency transition.

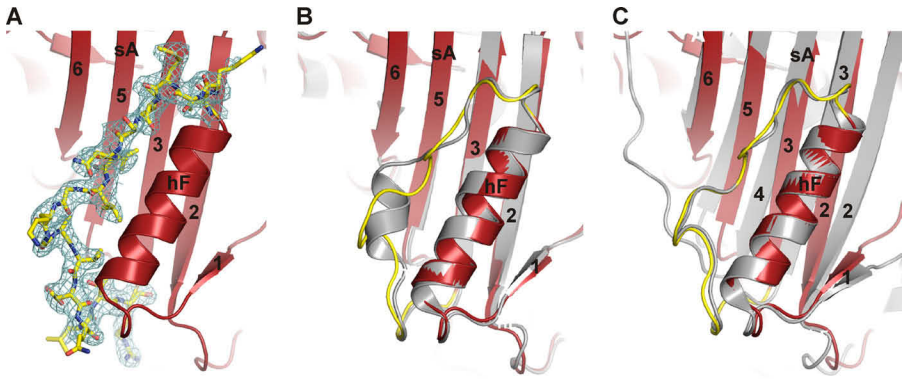

FIGURE 5. **Close-up view of the hF loop region consisting of hF and the loop Thr^{144}–Arg^{162} connecting hF with s3A.** All of the figures contain the W175F structure in a *red* cartoon presentation with the connecting loop highlighted in yellow. *A*, the residues in loop Thr^{144}–Arg^{162} are emphasized in stick presentation with the corresponding electron density at a sigma level of 1.0 in the $2F_o - F_c$ map. *B*, overlaid with the active 14-1B (*gray*, PDB code 1DVM). *C*, overlaid with the latent PAI-1 (*gray*, PDB code 1LJ5). All of the alignments are by direct alignment of the hF loop regions. α-hF and strands 1–6 of β-sheet A (*sA*) are labeled.

connecting s3B with hG, blocking the gate and thereby delaying latency transition (Fig. 4).

Salt Stabilization Occurs with Wild Type and W175F PAI-1—To support that a functional chloride site is found in both wild type and W175F PAI-1, we evaluated the stabilizing effect of high NaCl concentrations and showed this feature to be conserved between the two forms of PAI-1. This was demonstrated using standard latency transition assays performed at 37 °C (supplemental Fig. S2). The observed half-lives for the decay of inhibitory activity in the presence of 150 mM NaCl were ~49 and ~199 min for wild type and W175F PAI-1, respectively, consistent with observed variations of measured half-lives depending on buffer composition and experimental conditions (data not shown). Furthermore, both wild type and W175F PAI-1 exhibit a marked stabilization upon increasing the NaCl concentration to 1.0 M. A less than 10% drop in protease inhibition was observed over a 7-h time frame, yielding rough estimates of half-lives well above 30 h (>1800 min).

Stabilization Is Specific to Chloride Ions—To test the specificity of halide binding in the observed chloride-binding site, we performed similar kinetic stabilization studies using NaF and NaBr. In the presence of a 150 mM concentration of either NaF or NaBr, the inhibitory half-lives of wild type and W175F PAI-1 were similar to those measured in 150 mM NaCl (supplemental Table S2). In contrast to the dramatic stabilization observed with 1.0 M sodium chloride, the effects of the other halide salts are not as pronounced. A concentration of 1.0 M NaBr resulted in a modest stabilization, whereas a 1.0 M concentration of NaF yielded an intermediate level of stabilization of both PAI-1 variants. The stabilizing effect of NaF was only 1.9-fold for W175F PAI-1 and ~4-fold for WT PAI-1 in contrast to the >10- and >36-fold effect of NaCl in the same assay (supplemental Table S2).

Mapping Structural Differences by Statistical Approaches— To perform reliable structural comparisons between active and inactive PAI-1 conformations, we used the flexible alignment program RAPIDO (23). RAPIDO takes advantage of a genetic algorithm developed to create accurate comparisons of structures by taking the difference in statistical error into account. This is of utmost importance when comparing structures of different resolution and data quality (24), factors that directly affect the quality and resulting interpretations drawn from such alignments. Alignment of W175F with active 14-1B (PDB code 1DVM) (12) (Fig. 2) identified numerous structural differences.

The Most Prominent Structural Difference Is in the Helix F Loop Region—An important difference is observed in the region containing hF and the adjacent loop connecting hF to s3A, termed the hF loop region. The markedly increased functional as well as structural stability of 14-1B has been credited to clustering of three (N150H, K154T, and Q319L) of the four mutations in and below the loop connecting α-helix F (hF) with strand 3 in β-sheet A (s3A) (9). The clustering of these mutations induces a 3_{10}-like helix observed in all but one available structure of active 14-1B (Fig. 5*B*). The one interesting exception is observed when 14-1B is complexed with the N-terminal domain of vitronectin. In this complex the hF loop region reverts to a conformation close to that observed in W175F (25), in which the 3_{10} helix was not observed.

Widespread Conformational Differences—The differences observed in the alignment of W175F and 14-1B PAI-1 reveal the consequences of mutations in 14-1B and extensive relayed conformational changes (Fig. 2). One consequence of these mutations is a slight clockwise twist of hF that transmits a further structural change through movement of s1A. Moreover, there is a direct contact between the top part of hF and the loop between hD and s2A termed the "W86 loop," *i.e.* a salt bridge between Lys^{145} and Asp^{90}. This interaction is not observed in the W175F structure. These changes together perturb the conformation of the W86 loop and the position of hD in 14-1B as compared with the other structures. The combined effects of the conformational change of the W86 loop and the rearrangement of hD confer a noteworthy change in β-sheet A in which s2A and s3A are observed to be markedly shorter in W175F compared with 14-1B. Finally, a large conformational change is found on the "back" of the structure (Fig. 2), where hH and hG both shift toward the observed chloride-binding site. Interestingly, the mobility of these two helices suggests an intramolecular communication between the gate region and s2C, the position from which s1C adjacent to the RCL detaches before passing through the gate during latency transition.

DISCUSSION

As a member of the serpin superfamily, PAI-1 shares common structural features with others in the family. Specifically, the serpins are comprised of a core fold containing three β-sheets and several α-helices, with the RCL protruding from the core and accessible to target proteases. A unique feature of serpins is that their native forms are "metastable" because the exposed RCL is not in its most stable conformation. The mobility of the RCL is the feature that guides the inhibitory activity of serpins, and the RCL inserts readily into the central β-sheet upon cleavage by proteases and formation of a covalent acyl-intermediate. The driving force for this conformational change is thermodynamic, yielding a more stable and more extensive central β-sheet.

W175F PAI-1 Offers a Model of Native PAI-1—With PAI-1, this insertion of the RCL into the central β-sheet occurs readily, even without an interaction with target proteases, yielding a latent conformation that is inactive. Although serpins are all characterized by the metastable nature of the active conformation, the latency conversion for most is quite slow. In contrast, the conversion to the latent conformation occurs readily with PAI-1, with a half-life of only ~1 h at 37 °C. This facile relaxation of PAI-1 to the latent form has hampered structural determination of the metastable active protein. The main force driving the structural rearrangement of PAI-1 during protease inhibition and latency transition is the large thermodynamic energy difference between the active conformation and the more stable RCL-inserted forms. Here we confirm published data showing that the functional stabilization of 14-1B PAI-1 is also accompanied by a large increase in thermodynamic stability (Fig. 1), whereas W175F PAI-1 has thermodynamic stability comparable with that of wild type PAI-1. The determination of the x-ray crystallographic structure of W175F PAI-1 thus provides a more relevant structure for the metastable active form.

Structural Changes Are Apparent near the Vitronectin-binding Site in the Flexible Joint Region—Several structural features of W175F differ from the well characterized 14-1B form, which is dramatically stabilized so that it has lost most of its metastable character. A binding partner for PAI-1 that exists in high concentrations in plasma and tissues is vitronectin. Association of PAI-1 with vitronectin stabilizes the active conformation and significantly slows the latency transition. The complex of the N-terminal somatomedin B domain from vitronectin and PAI-1 has been determined (25), revealing a binding site in PAI-1 that is known as the flexible joint region in the vicinity of β-strands 1A, 2A, and 3A and the nearby helices D and E. The previously determined structure for the constitutively active 14-1B form of PAI-1, which has been the prior reference structure for the "active" form of PAI-1, contains four mutations, three of which are in the vicinity of this flexible joint region. Strikingly, the most notable structural differences comparing the W175F and 14-1B structures are proximal to this region. Notably, the loop connecting hF with strand 3A spanning the flexible joint region is missing a 3_{10}-helix that is observed in the 14-1B structure. Such a difference near the binding region for the key regulatory protein vitronectin makes the W175F PAI-1 structure preferred for ongoing studies on vitronectin-PAI-1 interactions.

The Helix F Loop Region Is Likely to Move as an Independent Domain—The conformation of the hF loop region in W175F closely mimics the conformation observed in the latent (9) (Fig. 5*C*) and the cleaved (26) (not shown) structures of PAI-1. The fact that the fold in the hF loop region is invariant between the active W175F and the latent structure indicates that this region behaves as an independent unit that remains unaffected by the major structural rearrangements in the remainder of the PAI-1 molecule during the insertion of the additional β-strand into sheet A (Fig. 5*C*). This observation supports the idea that the hF loop region moves as a rigid unit to allow space for the insertion of the RCL (27).

Other Structural Differences Distinguish the Metastable and Constitutively Active Structures—In the work described by Blouse *et al.* (17), in which W175F PAI-1 was generated, the exchange to phenylalanine was hypothesized to slow early preinsertion of the RCL prior to latency transition. In support of the importance of the area around position 175 is the model that includes an intermediate form of active wild type PAI-1 with a partially inserted RCL, a form termed the "prelatent" form (13, 14, 28, 29). Although no direct structural evidence exists for this prelatent form of PAI-1, it is thought to resemble what is observed for native antithrombin (30) in which the first few N-terminal residues of the RCL are inserted into a partially open β-sheet A, with the conformation of the breach region resembling what was observed for the structures of both the latent (PDB code 1LJ5) and cleaved (PDB code 3CVM) PAI-1.

Our new structure for W175F PAI-1 reveals shorter lengths observed for s3A and s2A that could facilitate the early stages of preinsertion. Although this is not direct proof, the structure would favor the ease of preinsertion and would thereby speed up RCL insertion, consistent with the relative fast decay of inhibitory activity of both wild type and W175F PAI-1 as compared with the slow transition of 14-1B. Furthermore, evidence from other serpins indicates the area spanning the top of s2A, s3A, and the connection to hD to be an important regulatory element by which cofactor binding to hD and hE influences the conformation of the RCL and thereby the reactivity of the serpins toward target proteases (30, 31). Our structural analysis also provides an explanation for why a conformationally sensitive antibody that recognizes the W86 loop preferentially binds to wild type active PAI-1 over active 14-1B (14). This W86 loop is significantly different between our structure and the structure of 14-1B (data not shown). Specifically, the bulky side chain of W86 protrudes into the solvent in our structure, whereas it points inwards and is buried inside the structure of 14-1B. From these comparisons, we conclude that the four point mutations in 14-1B result in widespread conformational differences (Fig. 1) that apparently lead to a general higher conformational rigidity of 14-1B.

The region around the single substituted residue Phe^{175} reveals no significant changes in the backbone conformation when compared with 14-1B (PDB code 1DVN) and a relatively modest shift when compared with the latent conformation (PDB code 1DVM) of PAI-1. Nonetheless, the side chain at position 175 occupies the same site, which presumably exhibits

complementarity and high affinity for aromatic side chains (Fig. 4, *C* and *D*). The mechanism that results in the mere 3.6-fold slower latency transition in the W175F mutant thus appears to result from local effects caused by the substitution of the Trp side chain by Phe, which increases the activation energy for RCL insertion rather than inducing global structural changes and stabilization as observed for 14-1B. Taken together, the differences between the W175F and 14-1B PAI-1 structures harbored in key regions for vitronectin binding and affecting the length of S2A and S3A, with minimal changes at the site of the mutation, indicate that the W175F structure represents a new unbiased model for the native active fold of the PAI-1 molecule.

The Chloride-binding Site in the Gate Region Accounts for the Stabilizing Effect of Salt—The hypothesis that the salt-dependent stabilization of PAI-1 activity is caused by a specifically bound chloride atom was originally proposed by Stout *et al.* (12). Although our new data support this hypothesis, the originally proposed location of the binding site in the 14-1B structure close to the hF loop region (Fig. 2) is not observed in our structure. It appears that the original binding site was indeed an artifact resulting from the induced conformational changes in the hF loop region caused by three of the four mutations in 14-1B. The effects of halide salts on stability were studied in the work published by Stout *et al.* (12), and a preferential stabilization was observed, with fluorine exhibiting the greatest effect followed by chlorine, bromine, and iodine, respectively. These studies were performed at a single time point following incubation of PAI-1 at either 37 °C or room temperature in a 150 mM halide concentration. Our studies comparing chlorine, bromine, and fluorine effects on stability, extended to include both wild type and W175F PAI-1, measured half-lives by taking measurements over an extended time frame rather than titrating tPA with PAI-1 at a single incubation time point. Nonetheless, our studies do not show any significant differences at the 150 mM concentration. Instead, pronounced differences in half-lives are observed at a 1.0 M sodium halide concentration, with chloride clearly giving the highest degree of stabilization of PAI-1. The reason for the differing results is not clear. We note that the halide salts had effects on the amidolytic activity of tPA and that controls for these effects were required for an accurate half-life determination for PAI-1.

Even though the crystals were grown at salt concentrations above those observed *in vivo*, it is likely that chloride-binding site will be observed under *in vivo* conditions. As seen in Fig. 4*B*, the chloride-binding pocket is disrupted in the latent form of PAI-1 because of rearrangements caused by the movement of secondary structural elements when β-sheet A expands upon RCL insertion. The former strand s1C, extracted from β-sheet C during latency transition, now stretches through the gate region as an extended loop precluding Cl^- binding. In summary, the new data provide a plausible and simple explanation for the stabilizing effect of salt as reviewed by De Taeye *et al.* (4). Our data support the proposed mechanism of chloride stabilization (12) but add a crucial correction of the actual location of the chloride-binding site to a location more directly linked to the observed retardation of latency transition. Furthermore, comparison of latency transition with other halide salts demonstrated a specific chloride effect. As the halide ion radii decreasing from fluorine to iodine, it appears that Cl^- must be the optimal size to bind with highest affinity to the site. Because chloride is the most abundant anionic ion under physiological conditions, this seems reasonable and suggests that this chloride site has a relevant physiological function.

The Divalent Metal Sites—The fact that two divalent cation sites are found in the crystal structure (Fig. 3) was surprising because no metal ions were added intentionally to the crystallization drops. Thus, the metals appear to associate with the protein either during purification or from trace elements present in the high salt concentration crystal conditions. It is debatable whether one or both of the metal sites are opportunistic, because they are present only at the dimer interface of the asymmetric unit. It thus remains an open question at which stage the metal ions are bound. The Zn^{2+} site at the N terminus of molecule chain A provides a plausible explanation for the fact that monomeric PAI-1 can be purified by divalent cation affinity chromatography without the use of specific protein tags (34). It is feasible that the metal chelating carboxyl groups of a metal-chelating Sepharose resin replace the metal ion coordination of Glu^{212} in chain A (Fig. 3), thereby mediating binding of PAI-1 through the two N-terminal histidine residues. It should be noted that adding submicromolar concentrations of either divalent zinc or copper ions to the crystallization drops caused immediate precipitation, supporting a specific interaction of the metals with PAI-1. This specific metal binding that leads to a conformational change may be relevant to recently published work that shows a destabilization of the active conformation of PAI-1 by copper, nickel, or cobalt and metal effects that are modulated by vitronectin binding to PAI-1 (32, 33).

Conclusion—The initial and final structures of latency transition are now well described by our x-ray crystal structure of the metastable active PAI-1 W175F and the latent wild type PAI-1 structure (PDB 1LJ5). This structure for W175F reveals differences in secondary structural elements in the breach region and the region involving Helix F and the loop connecting to s3A in the underlying central β-sheet. Thus, our present structure of W175F PAI-1 has revealed important differences from the 14-1B structure in the very region that houses three of the four mutations that appear to lead to the thermostability of the 14-1B form. Furthermore, the change in structure is found near the flexible joint region that constitutes the binding site for the somatomedin B domain from vitronectin, a cofactor that regulates the novel latency transition of PAI-1. A change in such a key region for PAI-1 function substantiates the need for a structure that more closely represents the active metastable form of PAI-1. Clearly, the movement of individual residues and individual secondary structural elements during the latency transition still remains to be established. With these new insights, the structure of W175F PAI-1 provides an improved and updated model of active PAI-1 that will better guide mapping of interaction surfaces, molecular mechanics, and *in silico* modeling.

Acknowledgments—Christine R. Schar is thanked for critical reading of the manuscript. We also express gratitude for beamline support by Santosh Panjikar and Andrea Smith (X12, EMBL Hamburg) and Clemens Schulze-Briese (Swiss Light Source) for making our experiments possible.

REFERENCES

1. Dupont, D. M., Madsen, J. B., Kristensen, T., Bodker, J. S., Blouse, G. E., Wind, T., and Andreasen, P. A. (2009) *Front. Biosci.* **14,** 1337–1361
2. Gils, A., and Declerck, P. J. (2004) *Thromb. Haemost.* **91,** 425–437
3. Andreasen, P. A. (2007) *Curr. Drug. Targets* **8,** 1030–1041
4. De Taeye, B., Gils, A., and Declerck, P. J. (2004) *Thromb. Haemost.* **92,** 898–924
5. Ye, S., Cech, A. L., Belmares, R., Bergstrom, R. C., Tong, Y., Corey, D. R., Kanost, M. R., and Goldsmith, E. J. (2001) *Nat. Struct. Biol.* **8,** 979–983
6. Huntington, J. A., Read, R. J., and Carrell, R. W. (2000) *Nature* **407,** 923–926
7. Mottonen, J., Strand, A., Symersky, J., Sweet, R. M., Danley, D. E., Geoghegan, K. F., Gerard, R. D., and Goldsmith, E. J. (1992) *Nature* **355,** 270–273
8. Berkenpas, M. B., Lawrence, D. A., and Ginsburg, D. (1995) *EMBO J.* **14,** 2969–2977
9. Sharp, A. M., Stein, P. E., Pannu, N. S., Carrell, R. W., Berkenpas, M. B., Ginsburg, D., Lawrence, D. A., and Read, R. J. (1999) *Structure Fold Des.* **7,** 111–118
10. Gettins, P. G. (2002) *Chem. Rev.* **102,** 4751–4804
11. Nar, H., Bauer, M., Stassen, J. M., Lang, D., Gils, A., and Declerck, P. J. (2000) *J. Mol. Biol.* **297,** 683–695
12. Stout, T. J., Graham, H., Buckley, D. I., and Matthews, D. J. (2000) *Biochemistry* **39,** 8460–8469
13. Hägglöf, P., Bergström, F., Wilczynska, M., Johansson, L. B., and Ny, T. (2004) *J. Mol. Biol.* **335,** 823–832
14. Li, S. H., Gorlatova, N. V., Lawrence, D. A., and Schwartz, B. S. (2008) *J. Biol. Chem.* **283,** 18147–18157
15. Minor, K. H., Schar, C. R., Blouse, G. E., Shore, J. D., Lawrence, D. A., Schuck, P., and Peterson, C. B. (2005) *J. Biol. Chem.* **280,** 28711–28720
16. Schar, C. R., Blouse, G. E., Minor, K. H., and Peterson, C. B. (2008) *J. Biol. Chem.* **283,** 10297–10309
17. Blouse, G. E., Perron, M. J., Kvassman, J. O., Yunus, S., Thompson, J. H., Betts, R. L., Lutter, L. C., and Shore, J. D. (2003) *Biochemistry* **42,** 12260–12272
18. Lawrence, D. A., Olson, S. T., Palaniappan, S., and Ginsburg, D. (1994) *Biochemistry* **33,** 3643–3648
19. Kabsch, W. (2010) *Acta Crystallogr. D Biol. Crystallogr.* **66,** 125–132
20. (1994) *Acta Crystallogr D. Biol. Crystallogr.* **50,** 760–763
21. Adams, P. D., Afonine, P. V., Bunkóczi, G., Chen, V. B., Davis, I. W., Echols, N., Headd, J. J., Hung, L. W., Kapral, G. J., Grosse-Kunstleve, R. W., McCoy, A. J., Moriarty, N. W., Oeffner, R., Read, R. J., Richardson, D. C., Richardson, J. S., Terwilliger, T. C., and Zwart, P. H. (2010) *Acta Crystallogr D Biol. Crystallogr* **66,** 213–221
22. Emsley, P., and Cowtan, K. (2004) *Acta Crystallogr D* **60,** 2126–2132
23. Mosca, R., Brannetti, B., and Schneider, T. R. (2008) *BMC Bioinformatics* **9,** 352
24. Schneider, T. R. (2002) *Acta Crystallogr D Biol. Crystallogr* **58,** 195–208
25. Zhou, A., Huntington, J. A., Pannu, N. S., Carrell, R. W., and Read, R. J. (2003) *Nat. Struct Biol.* **10,** 541–544
26. Jensen, J. K., and Gettins, P. G. (2008) *Protein Sci.* **17,** 1844–1849
27. Gettins, P. G. (2002) *FEBS Lett.* **523,** 2–6
28. Verhamme, I., Kvassman, J. O., Day, D., Debrock, S., Vleugels, N., Declerck, P. J., and Shore, J. D. (1999) *J. Biol. Chem.* **274,** 17511–17517
29. Gorlatova, N. V., Elokdah, H., Fan, K., Crandall, D. L., and Lawrence, D. A. (2003) *J. Biol. Chem.* **278,** 16329–16335
30. Johnson, D. J., Langdown, J., Li, W., Luis, S. A., Baglin, T. P., and Huntington, J. A. (2006) *J. Biol. Chem.* **281,** 35478–35486
31. Chuang, Y. J., Swanson, R., Raja, S. M., Bock, S. C., and Olson, S. T. (2001) *Biochemistry* **40,** 6670–6679
32. Thompson, L. C., Goswami, S., Ginsberg, D. S., Day, D. E., Verhamme, I. M., and Peterson, C. B. (2011) *Protein Sci.* **20,** 353–365
33. Thompson, L. C., Goswami, S., and Peterson, C. B. (2011) *Protein Sci.* **20,** 366–378
34. Day, D. D. (March 21, 2006) U. S. Patent 7,015,021 B2